Werk

Jahr: 1980
Kollektion: fid.geo
Signatur: 8 Z NAT 2148:48
Digitalisiert: Niedersächsische Staats- und Universitätsbibliothek Göttingen
Werk Id: PPN1015067948_0048
PURL: http://resolver.sub.uni-goettingen.de/purl?PPN1015067948_0048

LOG Id: LOG_0023
LOG Titel: Source parameters of earthquakes from the Himalayan region
LOG Typ: article

Übergeordnetes Werk

Werk Id: PPN1015067948
PURL: http://resolver.sub.uni-goettingen.de/purl?PPN1015067948
OPAC: http://opac.sub.uni-goettingen.de/DB=1/PPN?PPN=1015067948

Contact

Niedersächsische Staats- und Universitätsbibliothek Göttingen
Georg-August-Universität Göttingen
Platz der Göttinger Sieben 1
37073 Göttingen
Germany
Email: gdz@sub.uni-goettingen.de

J. Geophys. 48, 67–79, 1980

Journal of Geophysics

Source Parameters of Earthquakes From the Himalayan Region*

S.K. Upadhyay[1] and S.J. Duda[2]

[1] Department of Earth Sciences, University of Roorkee, Roorkee, U.P., India

[2] Institut für Geophysik, Universität Hamburg, Bundesstraße 55, D-2000 Hamburg 13, Federal Republic of Germany

Abstract. Source parameters of eight recent earthquakes from the Himalayan region are investigated, using single station digital data from the Central Seismological Observatory in Erlangen (FRG). Spectral displacement densities are obtained for both *P*- and *S*-waves and compensated for the effects of geometrical spreading and the instrument response in the applicable frequency range. Consideration is given to the effects of anelasticity and the radiation pattern. The compensated spectral densities are analysed in terms of theoretical faulting models. The seismic moment, the fault length and area, the stress drop and related quantities are estimated. Some evidence is presented as to the source time function and the anelasticity of the area.

Only one half of the earthquakes analysed are found to comply with the one-corner frequency model, the remaining earthquakes revealing two corner frequencies. The source time function as retrieved from the far field displacement shows approximately a cubic increase with time ($t^3 \exp(-vt)$). The earthquakes are found to be of the low stress drop/low moment type.

Key words: Earthquake source models – Seismic moment – Stress drop – Source time function – Himalaya region.

Introduction

Following Reid's (1910) 'Elastic Rebound Theory', various models have been proposed for the description of the process in the earthquake focus. The approaches can be classified as static and as kinematic. In the first case earthquakes are treated as the solution of a problem of elastostatics. Here no consideration is given to the action of inertial forces, and attention is stressed on the permanent deformation incurred subsequently to the earthquake process in the medium surrounding the focus. The empirical verification of such models resorts primarily to geodetic measurements of deformation around faults. The components of the strain tensor can then be determined and related to the seismic moment, the fault dimension, the stress drop and the seismic energy of earthquakes (e.g., Tsuboi 1939; Byerly and De Noyer 1958; Chinnery 1961, 1963). In practice, this approach is restricted to observations made at short epicentral distances and to near-surface events.

On the other hand, in kinematic models of the earthquake process, the inertial forces are taken into account and the earthquake is treated as the solution of a boundary value problem. In addition to the source parameters previously mentioned, new parameters enter the problem, as the polarisation angle of *S*-waves, the sense of first *P*-wave motion, the rupture velocity, the friction on the fault planes and the source time function. Thereby the source parameters are, at least in principle, retrievable from the seismograms of earthquakes.

Kinematic models have received considerable attention in recent years, due to the greater flexibility of the approach, and due to the relative ease of making observations at both small and large epicentral distances. In line with this approach the present paper is based on the analysis of seismograms for the purpose of obtaining source parameters of a suit of earthquakes from a particular region – the Himalayas.

Mathematically treatable source models assume either a displacement discontinuity across the fault plane (e.g., Haskell 1964, 1966, 1969; Savage 1966; Aki 1967), or a stress discontinuity due to a distribution of elementary forces acting at each point of the fault plane (e.g., Ben-Menahem 1962; Hirasawa and Stauder 1965). The source time function, i.e., the displacement or stress at each point of the fault plane as function of time, has been originally postulated to have the form of either a step (Aki 1968), or a ramp (Haskell 1964). Brune (1970) related – more realistically – the source time function to the effective stress available to accelerate the two sides of the fault.

On this basis, the aims of the present paper are the following:

(i) verification of known theoretical earthquake models with the help of eight well-recorded earthquakes from the Himalaya-region,

(ii) retrieval of the source parameters, and

(iii) analysis of the source time function characteristic of the earthquakes.

Data and Method of Analysis

Digital magnetic tape recordings of the earthquakes listed in Table 1 were obtained at the Central Seismological Observatory (Gräfenberg) at Erlangen (FRG). The position of the earthquakes with respect to the observatory is shown in Fig. 1. *P*- and *S*-waves were analysed for time intervals of 40 and 80 s and of 60 and 120 s respectively, beginning at the expected arrival time of each of the waves. The time intervals determine the lowest usable frequency. On the other hand, the Nyquist frequency (10 Hz) is determined by the digitisation interval, amounting to 1/20 s. Displacement amplitude spectral densities are obtained by way of the FFT-method. Corrections for the instrument response, the geometric spreading of the wave front and the effect

* The paper was prepared while Dr. Upadhyay stayed at the Institute of Geophysics of Hamburg University, as awardee of a fellowship of the A.v.Humboldt-Foundation

0340-062X/80/0048/0067/$02.60

Table 1. List of earthquakes analyzed

Earthquake No.	Date	Origin time	Magnitude[a] M_B	Magnitude[a] M_S	Depth (km)	Location of epincentre	Epicentral distance from Central Seismological Observatory	Source azimuth from Central Seismological Observatory
1	29.5.76	$12^h\,23^m\,18.7^S$	6.1	6.9	8	24.57° N 98.953° E	70.11°	75.103°
2	29.5.76	$14^h\,00^m\,18.5^S$	6.0	7.0	10	24.531° N 98.71° E	69.98°	75.303°
3	12.8.76	$23^h\,26^m\,46.2^S$	6.4	5.8[b]	27	26.68° N 97.07° E	67.41°	74.847°
4	6.11.76	$18^h\,04^m\,08.9^S$	5.8	6.5	33	27.605° N 101.05° E	69.21°	71.415°
5	21.7.76	$15^h\,10^m\,45.6^S$	5.8	6.3	9	24.782° N 98.698° E	69.79°	75.123°
6	9.6.76	$00^h\,20^m\,39.5^S$	5.7	5.9	33	24.894° N 98.752° E	69.75°	75.007°
7	1.1.77	$21^h\,39^m\,41.3^S$	5.9	6.3	27	38.146° N 91.007° E	55.86°	69.240°
8	19.1.77	$0^h\,46^m\,18.3^S$	5.9	5.8	33	37.022° N 95.697° E	59.42°	67.383°

Coordinates of recording station of the Central Seismological Observatory: 49° 41′ 31″ N, 11° 13′ 18″ E;

[a] Magnitudes published by USGS, unless otherwise mentioned

[b] Magnitude calculated from Erlangen records

of the free surface are introduced into the spectra by way of well-known methods (see Båth 1974). The velocity response of the instruments of the Central Seismological Observatory is shown in Fig. 2.

It may be mentioned that the earthquakes investigated are the strongest in the region under consideration, in recent time. Furthermore, it has been made sure that no microseismic storm took place during any of the earthquakes. In consequence of that, and in view of the quality of the recording station, the signal-to-noise ratio is as favourable as it can be for respective earthquakes observed in Central Europe.

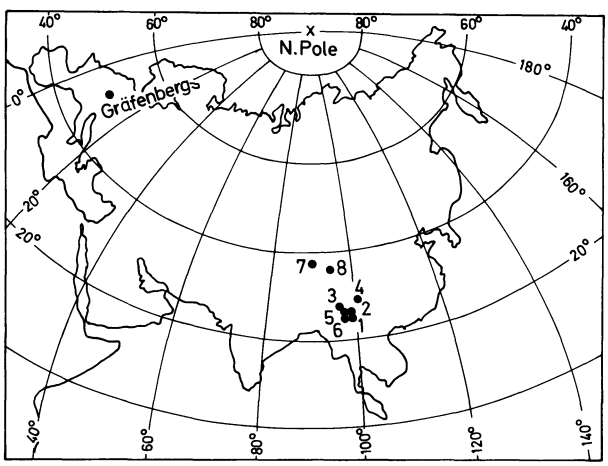

Fig. 1. Position of the epicentres in the Himalayan region with respect to the recording station. *Numbers* adjacent to the epicentre locations correspond to those used in the remaining figures and tables

Theory

The kinematic source models developed by Haskell (1964), Aki (1967), Berckhemer and Jacob (1968), Brune (1970) and Savage (1972) predict a far field radiation with the following common features:

(i) the low-frequency trend in the displacement density spectrum forms a line parallel to the frequency axis;
(ii) the displacement density spectrum decays at high frequencies;
(iii) the high-frequency and low-frequency trends in the spectrum intersect at one or at two frequencies, forming corners in the spectrum and defining corner frequencies;
(iv) corner frequencies are related to the dimensions of the source;
(v) the low-frequency value of the spectrum is determined by the seismic moment of the source;
(vi) the high-frequency decay of the spectrum is controlled by stress drop or by the effective stress (Brune 1970).

The following relations exist between the source parameters and the parameters characterising the displacement density spectrum of the radiated signal.

Seismic Moment M_0. According to Keilis-Borok (1959):

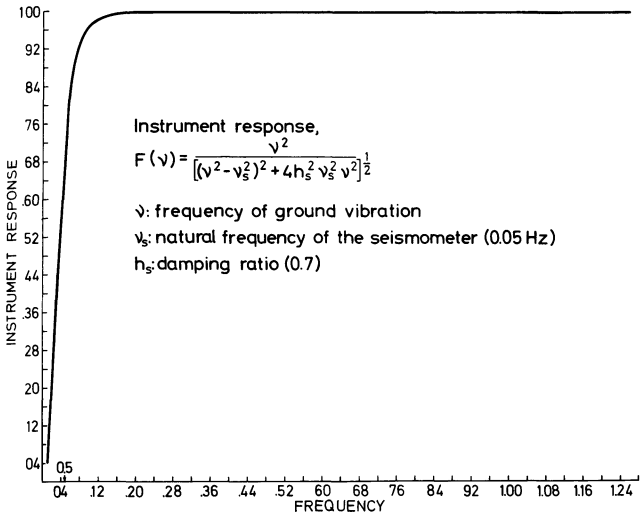

Fig. 2. Instrument response of seismometers used

$$M_0=\frac{4\pi\rho v^3\Omega_0(\omega)}{2RR_{\theta\phi}} \tag{1}$$

where

ρ = density near the seismic source, in gm/cm^3
R = factor accounting for the geometrical spreading of the wave front in a spherically stratified earth, in cm^{-1}
v = velocity of P- (α) and S-waves (β) in the source region, in cm/s
$\Omega_0(\omega)$ = low-frequency level of the displacement density spectrum, in cm/s
$R_{\theta\phi}$ = factor accounting for the radiation pattern of P- and of S-waves; $0\leqq|R_{\theta\phi}|\leqq 1$.

The amplification of the amplitude at the free surface is taken care of by the factor 2 in the denominator.

In Eq. (1) R is given by

$$R=\frac{1}{r_0}\left|\frac{\sin i_h}{\sin\Delta\cos i_0}\frac{di_h}{d\Delta}\right|^{\frac{1}{2}} \tag{2}$$

with

r_0 = radius of the Earth, in cm
i_h = angle of emergence at the focus at depth h of the ray emerging at epicentral distance Δ
i_0 = angle of incidence at the Earth's surface, at epicentral distance Δ (Shimshoni and Ben Menahem 1970).

Formula (1) is used for the determination of the seismic moment. For this purpose, in the present paper, the following numerical values are assumed for the respective quantities:

$\rho=2.7$ gm/cm^3
$\alpha=6.0$ km/s
$\beta=3.5$ km/s
$\mu=3.3\times10^{11}$ dynes/cm^2.

Fault Dimension. Formulae involving the fault dimensions have been derived for various source models. Depending on the model, the fault dimensions are functions of the corner frequency or frequencies f_i ($i=1,2,3$), the seismic velocities α, β at the focus, the rupture velocity v_R and the fractional stress drop ε. Table 2 shows the formulae for the models of Haskell (1964),

Table 2. Relation between corner frequencies f_i and fault dimensions for various fault models (Savage 1972)

Model	S-wave	P-wave
Haskell $\left(\frac{v_R}{\beta}=0.9\right)$		
One corner frequency:	$f_3=3.8\frac{\beta}{\sqrt{A}}$	$f_3=1.7\frac{\alpha}{\sqrt{A}}$
Two corner frequencies	$f_1=3.6\frac{\beta}{L}$	$f_1=1.2\frac{\alpha}{L}$
	$f_2=4.1\frac{\beta}{w}$	$f_2=2.4\frac{\alpha}{w}$
Brune ($L=2a$)		
One corner frequency	$f_3=4.1\beta\sqrt{\frac{1.6-0.6\varepsilon}{\varepsilon A}}$	$f_3=4.1\alpha\sqrt{\frac{1.6-0.6\varepsilon}{\varepsilon A}}$
Two corner frequencies	$f_1=4.7\frac{\beta}{L}$	$f_1=4.7\frac{\alpha}{L}$
	$f_2=4.7\frac{\beta}{L}\left(\frac{1.6-0.6\varepsilon}{\varepsilon}\right)$	$f_2=4.7\frac{\alpha}{L}\left(\frac{1.6-0.6\varepsilon}{\varepsilon}\right)$
Berckhemer and Jacob $\left(L=2a,\ \frac{v_{\max}}{\beta}=0.9\right)$		
One corner frequency	$f_3=2.5\frac{\beta}{L}$	$f_3=1.5\frac{\alpha}{L}$

v_R = average rupture velocity in cm/s. L, w, A = length (cm), width (cm) and area (cm^2) of fault, ε = (dimensionless) fractional stress drop. While Haskell assumes a rectangular model, both Brune, and Berckhemer and Jacob assume equivalent circular models (radius = a) of the fault. $f_3=\sqrt{f_1 f_2}$ applies

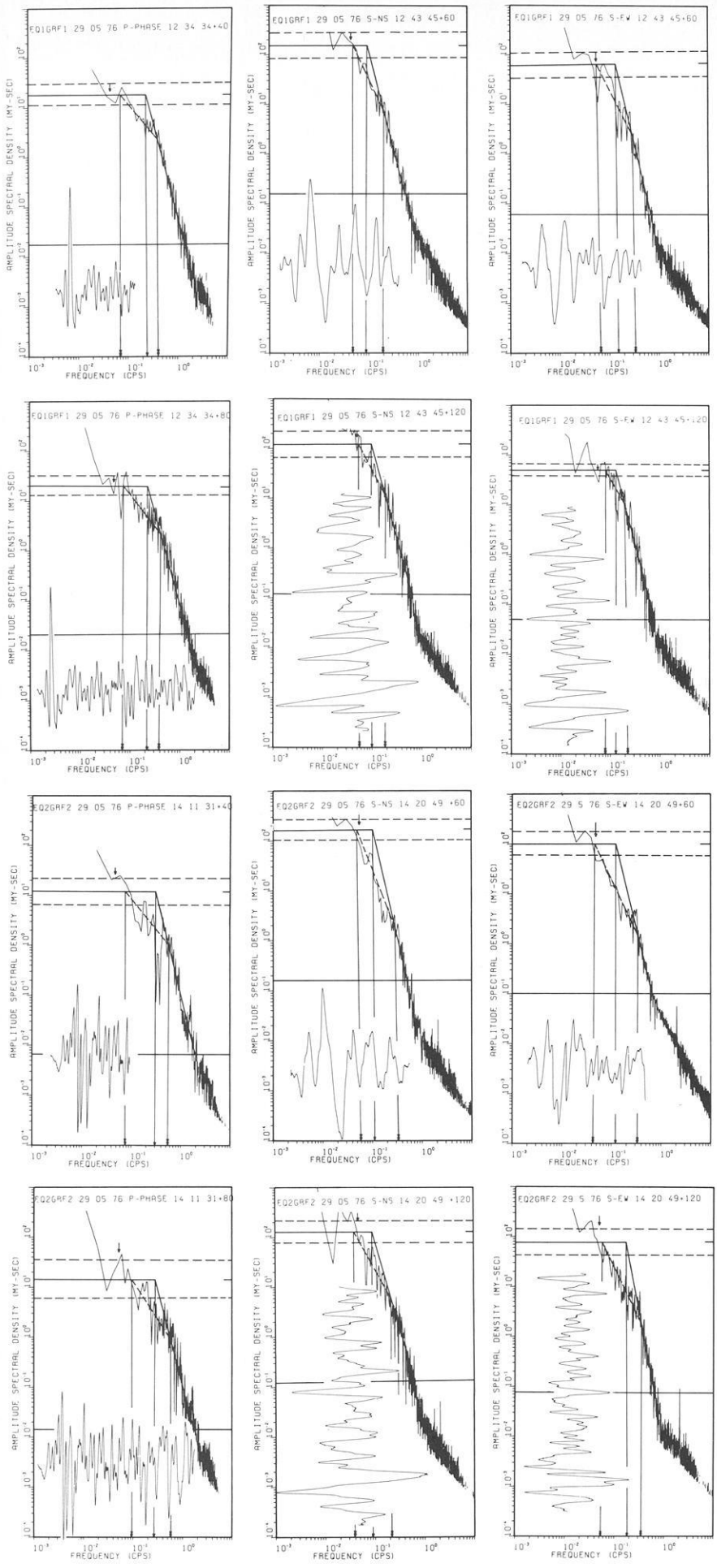

Fig. 3.
Seismograms and spectra corresponding to earthquakes No. 1 (upper portion) and No. 2 (lower portion).
Note: *P*-waves (vertical component) and N−S and E−W component of *S*-waves appear in the first, second and third column, respectively. For further explanation, refer to the text

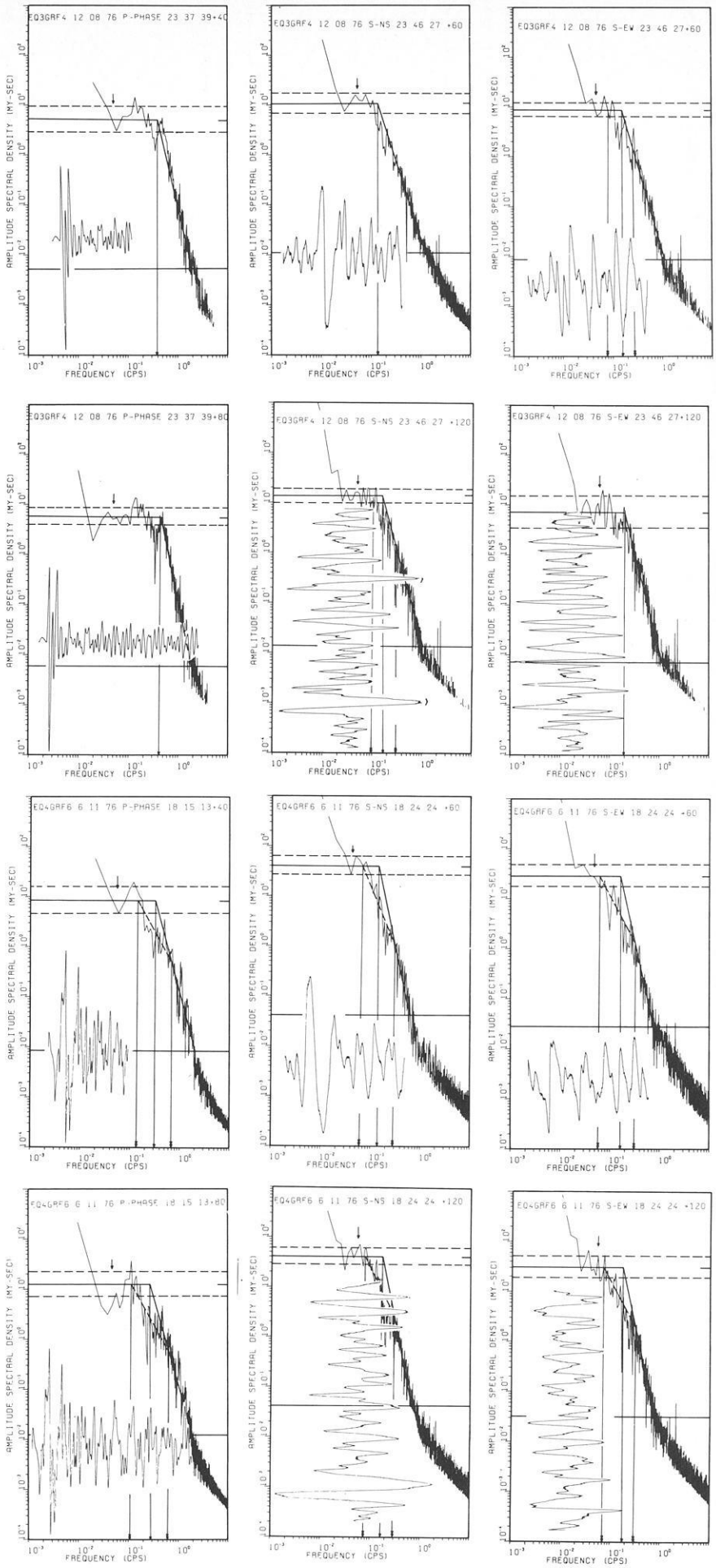

Fig. 4.
Seismograms and spectra corresponding to earthquakes No. 3 (upper portion) and No. 4 (lower portion). See Note of Fig. 3

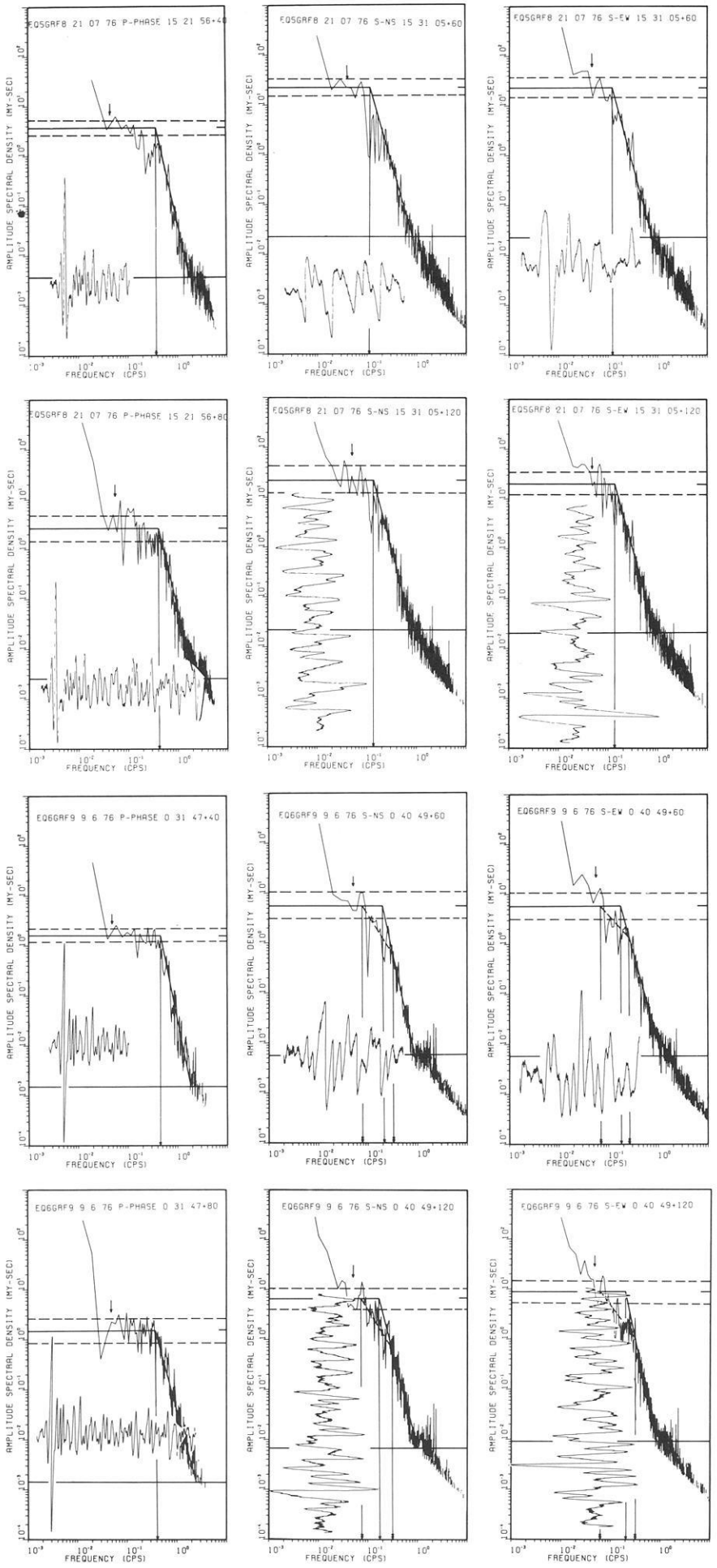

Fig. 5.
Seismograms and spectra corresponding to earthquakes No. 5 (upper portion) and No. 6 (lower portion). See Note of Fig. 3

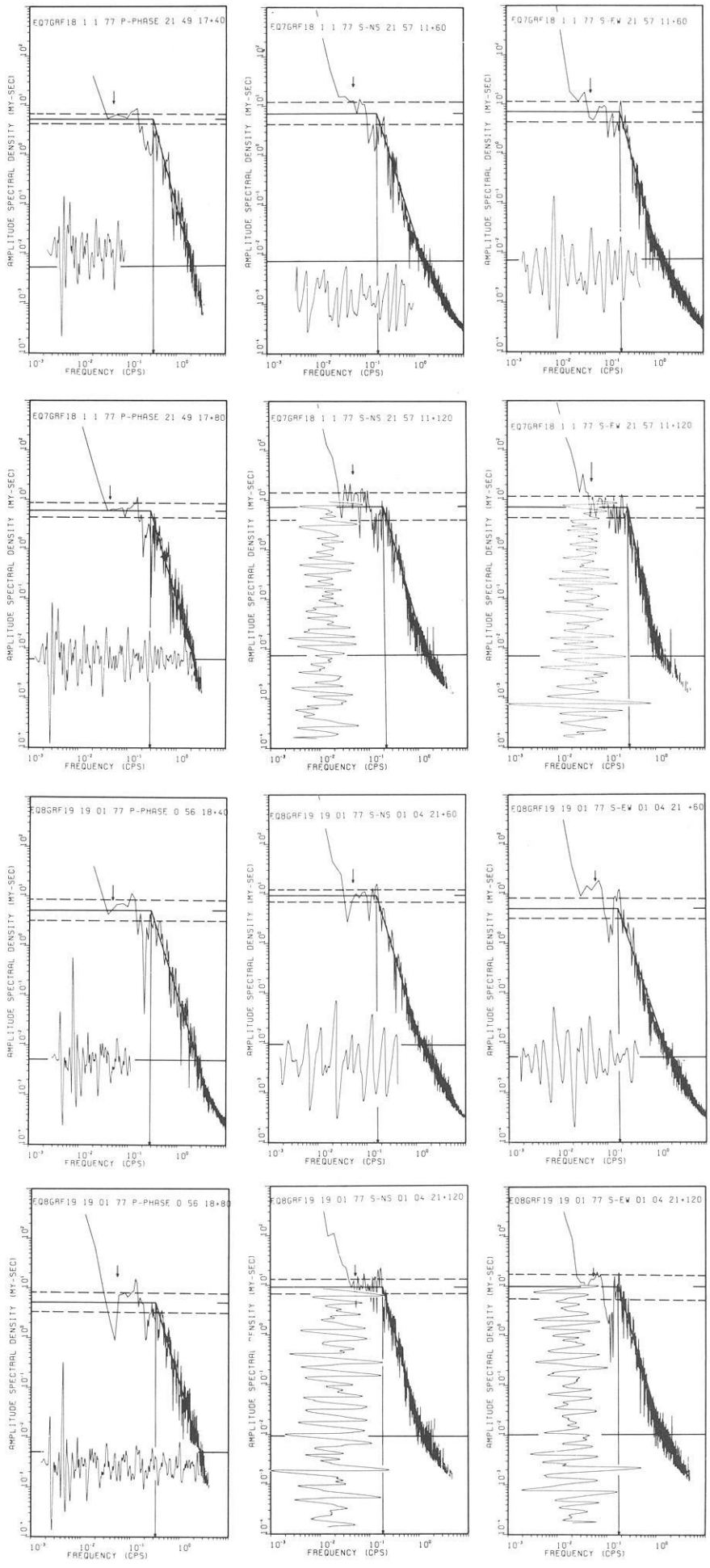

Fig. 6.
Seismograms and spectra corresponding to earthquakes No. 7 (upper portion) and No. 8 (lower portion). See Note of Fig. 3

Berckhemer and Jacob (1968), Brune (1970) and Savage (1972). In Haskell's model, the fault plane is assumed to be of rectangular shape, the width and length being ω and L respectively. Also, unilateral fracture propagation with a constant rupture velocity is here assumed. In Brune's model, the rupture propagation is neglected. Instead, the parameter ε is introduced which accounts for the fractional stress drop along the fault plane during the earthquake. In Berckhemer and Jacob's model, the effect of maximum reputure velocity, as opposed to average rupture velocities in the previous cases, is considered. In a generalisation of Haskell's (1964) model, a bilateral fracture propagation in opposite directions is discussed by Savage (1972). In this case, as also in Haskell's model, two corner frequencies are expected, provided that the ratio of fault length to width is large.

Average Dislocation and Stress Drop. Aki (1966) has related the seismic moment M_0 to the average dislocation $\bar{u}$, and the fault area A $(=L\cdot\omega)$ through the formula

$$\bar{u}=\frac{M_0}{\mu A} \tag{3}$$

where μ is the rigidity of the material in the earthquake focus. The seismic moment so found can be used for the estimation of the stress drop, $\Delta\sigma=(\sigma_1-\sigma_2)$, during an earthquake at the focus, whereby σ_1 and σ_2 are the average initial and final shear stresses on the fault surface respectively. According to Brune (1970) the corresponding relation for a circular fault plane with radius r is

$$\Delta\sigma=\frac{7}{16}\cdot\frac{M_0}{r^3}, \tag{4}$$

which readily can be estimated.

Structure of the Spectra and Numerical Results

Figures 3–6 show body wave displacement density spectra, corrected for the instrument response. Each of the graphs identifies in the top line the earthquake as to its number in Table 1, and the occurrence date, as well as the wave-type, the seismometer-component under consideration, the arrival time of the respective phase and the record length (40, 80 or 60, 120 s). The wave trains analysed are included in the lower left portion of each diagram. The arrow in the upper part of the diagrams indicates the frequency at which the response of the seismometer falls below 0.707 of the maximum value. Below this frequency the spectra become progressively less reliable. The steep rise of the spectra at the lowest frequencies is attributed to the truncation of the signal with a box car or Hamming window, in accordance with results of Linde and Sacks (1971). Nonetheless, a plateau is identified in all cases, though of variable quality. An approximation of the constant level and of the decaying part of the spectrum is attempted, as shown by the solid lines. The intersection of the two lines defines the corner frequency. Wherever applicable, the spectra are approximated by an additional, intermediate line (dashed). Two corner frequencies (f_1, f_2) are defined by the intersections of the dashed and the two solid (level and decaying) lines. The portion of the spectrum with values three decades below the level portion is neglected as a rule in the approximations. An error estimate of the level portion of the spectrum is indicated by horizontal, parallel lines (dashed) above and below the optimum value. The corner frequencies are shown by arrows on the frequency axis.

The spectra are found to have a definable constant level at low frequencies. The high frequency decay is controlled by one segment in case of the earthquakes Nos. 5, 7 and 8 yielding one corner frequency (type A earthquakes), and by two segments in case of earthquakes Nos. 1, 2, and 4 (type B earthquakes) yielding two corner frequencies. For earthquake No. 6, only the spectra of *S*-waves show two corner frequencies. Earthquake No. 3 yields spectra with one corner frequency though with two exceptions (*S*-wave on EW-(60 s) and NS-(120 s) components). Both earthquake Nos. 3 and 6 are labeled as type C (see Table 3).

The high-frequency decay of the spectra is approximated by the function const. $f^{-\gamma}$. Table 3 summarizes all pertinent values concerning the spectra. The values given in the table are averages of determinations made independently for the *P*-wave signals 40 and 80 s in length, and for the *S*-wave signals 60 and 120 s in length. For *S*-waves, the values from the two horizontal component records were averaged too. The respective corner frequencies as well as Ω_0 and $+\gamma$ revealed a good agreement, even prior to averaging (see Figs. 3–6), proving that these values are independent of the record length for a particular phase within the range investigated.

Table 4 gives the numerical values of the seismic moments, the stress drop and the average dislocation, as found with the formulae (1), (4), and (3), and the Table 2. Thereby, the moment from *S*-waves is obtained by way of a vector addition of the values found from the NS- and EW-component, as usually done. Also, for comparison, the seismic moments are given in accordance with the formula,

$$\log M_0 = M_S + 19.2 \tag{5}$$

valid in the magnitude range $6\leqq M_S\leqq 7$, with M_0 in dyne cm, and correlating the moment with the surface wave magnitude (Aki 1973). It can be seen that the moments of the 8 Himalaya-earthquakes determined from *S*- and from *P*-waves are in fair agreement, for each of the earthquakes, while at the same time they are lower on the average, by one order of magnitude, if compared with the ones found from Aki's formula.

The question arises as to the achievable accuracy of seismic moment determinations. In view of the difficulties in separating *P*- and *S*-phases from others, as *pP*, *sS*, *sP*, *pS*, core phases, etc., it is quite possible that the signals Fourier-analysed are the result of interference between phases. This can lead to an overestimate of the moment by a factor of 2–3. Thus, individual moment determinations can be accurate only to within about one order of magnitude. Even so, though, the deviation of moments of the Himalaya-earthquakes here investigated, from Aki's average relation appears to remain valid.

No clear dependence of either the stress drop or the average dislocation on magnitude is seen. All eight earthquakes feature however relatively small values of the stress drop, which fact labels the earthquakes as being of low stress drop type.

Table 4 further shows the fault length and area, as found from the spectra when using the three source models indicated. As a rule, the fault plane area found from *P*-waves is smaller than that from *S*-waves. In addition, differences among the estimates of upto one order of magnitude are seen, depending on the model employed. A comparison is made in Fig. 7 of all fault plane areas found here from *S*-waves, with fault plane areas given by Båth and Duda (1964) and by Chinnery (1969).

Table 3. Characteristics of displacement amplitude density spectra for *P*- and *S*-waves

Earthquake		Spectral characteristic of *P*-wave					Spectral characteristic of *S*-wave					
No.	Type	Ω_0 ($\times 10^{-4}$ cm-s)	$+\gamma$	f_1 (Hz)	f_2 (Hz)	f_3 (Hz)	Ω_0(NS) ($\times 10^{-4}$ cm-s)	Ω_0(EW) ($\times 10^{-4}$ cm-s)	$+\gamma$	f_1 (Hz)	f_2 (Hz)	f_3 (Hz)
1	B	19	3.47	0.07	0.39	(0.24)	150	55	4.57	0.061	0.23	(0.12)
2	B	14	3.92	0.086	0.57	(0.29)	150	89	4.52	0.047	0.30	(0.13)
3	C	5.65	4.49	–	–	0.41	12	8	3.75	0.075(?)	0.28(?)	(0.17)
4	B	10.25	3.61	0.13	0.65	(0.30)	40	30	3.82	0.065	0.29	(0.17)
5	A	3.15	4.33	–	–	0.40	22	22	3.66	–	–	0.13
6	C	1.6	4.33	–	–	0.41	6	7	4.27	0.071	0.30	(0.18)
7	A	5.65	3.47	–	–	0.30	7	7	4.38	–	–	0.22
8	A	5.1	3.14	–	–	0.30	9	7	3.86	–	–	0.18

γ = slope (negative) of high-frequency portion of spectrum
A = one corner frequency, *B* = two corner frequencies, *C* = mixed spectra – one or two corner frequencies

Table 4. Calculated values of seismic source parameters

Earthquake			Phase used	Moments		Stress drop (bars)	Average dislocation (cm)	Brune's model		Haskell's model			Berckhemer and Jacob's model	
No.	M[a]	Type[b]		Determined from spectra	from Aki (1973)			Length (km)	Area (km^2)	Length (km)	Width (km)	Area (km^2)	Length (km)	Area (km^2)
				$\times 10^{25}$	(dyne·cm)									
1	6.9	B	P	1.42	12.6	7.2	15.1	19	284	16	6	96	6	29
			S	2.05		3.6	12.8	24	451	33	10	324	12	106
2	7.0	B	P	0.80	15.8	8.5	14.5	15	168	13	4	54	5	19
			S	2.23		6.0	16.8	22	380	43	8	325	11	96
3	5.8	C	P	0.39	(1.0)	10.3	12.4	11	96	4		16	4	10
			S	0.18		3.3	2.9	16	189	27	8	218	8	53
4	6.5	B	P	0.69	5.0	7.1	11.8	15	177	9	4	31	5	18
			S	0.57		1.0	3.6	24	467	31	8	245	8	55
5	6.3	A	P	0.23	3.2	5.6	7.0	11	101	4		17	4	10
			S	0.39		1.3	3.9	20	305	16		272	11	87
6	5.9	C	P	0.10	(1.3)	2.9	3.3	11	96	4		16	3	10
			S	0.09		0.7	1.6	15	165	29	8	218	8	47
7	6.3	A	P	0.33	3.2	3.6	5.7	15	177	5		29	5	18
			S	0.10		1.7	2.6	12	113	10		95	6	31
8	5.8	A	P	0.32	(1.0)	3.0	5.3	15	184	5		29	5	19
			S	0.30		2.4	5.3	15	170	12		142	8	49

For one-corner frequency earthquake (Type A) Haskell's model predicts equal length and width of fault plane.
Moments outside of range of applicability of Aki's (5) formula are given in parantheses

[a] Compare Table 1
[b] Compare Table 3

The fault plane areas from the three models show a clear though gentle dependence on the surface wave magnitude. For the larger earthquakes, the areas are exceeded by those corresponding to Chinnery's, and to Båth and Duda's empirical formulae, while for the smaller magnitudes a better agreement of all estimates is found. This fact may bear some evidence concerning the strain release. The determination of the fault plane area by Båth and Duda was based on Benioff's hypothesis, according to which the aftershocks delineate the fault plane activated during the main shock. While this hypothesis is sup-

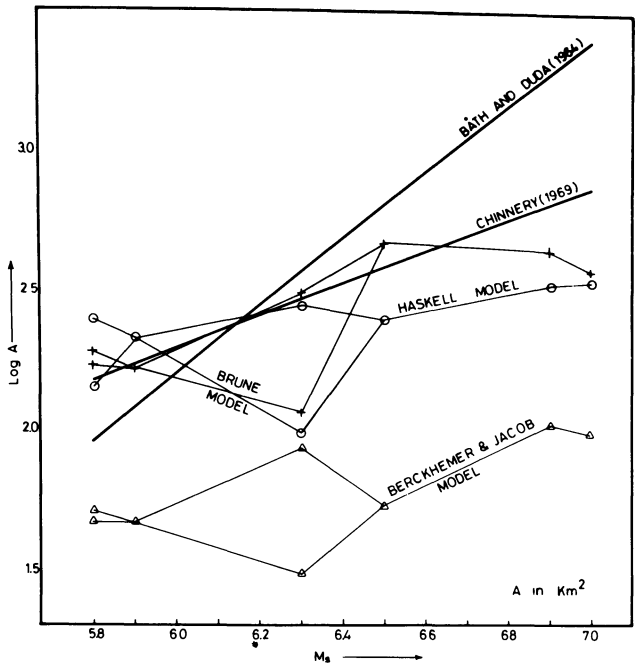

Fig. 7. Fault plane area as determined in the present study according to three different models of earthquake process. Included are results obtained earlier by different methods shown in *thick solid lines*

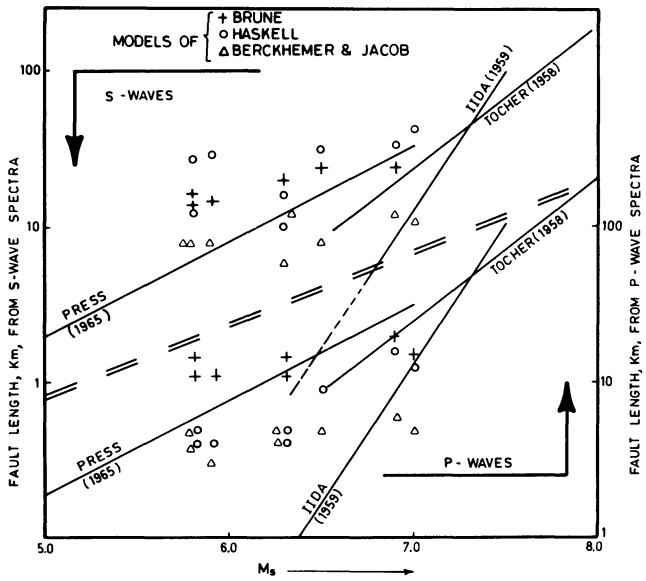

Fig. 8. Fault length from *S*-waves (upper portion) and from *P*-waves (lower portion) as determined in the present study according to three different models of the earthquake process. Included are the results obtained earlier by different methods shown by *solid lines*

ported by the present measurements only in the lower magnitude range, say from 5.8 to 6.4, it is contradicted for large magnitudes. In the latter range the main shock occurs on a smaller fault plane than is the plane delineated by subsequent aftershocks. The aftershocks let the originally activated fault plane grow, its area yielding an overestimate of the fault plane area of the main shock. This discrepancy of fault plane areas, as seen in Fig. 7 for magnitudes above 6.4, is viewed on the background of the relative abundance of aftershocks following the larger earthquakes. It indicates that the stress drop in a large magnitude main shock is less complete than in case of a main shock in the magnitude range, say, 5.8–6.4.

The disagreement of the Båth and Duda formula on one side, and the estimates of the fault plane area in the upper magnitude range on the other (Fig. 7), can also be a consequence of the fact that the coherence length K_L^{-1} and the coherence time K_T^{-1}, as defined by Aki (1967), are systematically exceeded by the fault length L and the characteristic time T. The possibility of an underestimate of the fault dimension under this condition was pointed out by Savage (1972). If this is the case, Benioff's hypothesis mentioned above continues to be valid in the entire magnitude range, along with Båth and Duda's fault plane formula.

Figure 8 compares the fault lengths found here from the three models, with empirical formulae which have been published by Tocher (1958), Iida (1959) and Press (1965). The estimates found in the present study are given separately for *P*- and for *S*-waves.

The formula by Iida shows the poorest agreement with the present results, while those by Tochter and Press appear to feature a too strong dependence on magnitude. The overall agreement of the results with the two empirical formulae is, however, satisfactory.

Discussion

Theoretical considerations lead to opposing views on the behaviour of seismic spectra at low frequencies. A constant level down to zero frequency is predicted in models of Haskell (1964), Aki (1967), Berckhemer and Jacob (1968), Brune (1970) and Savage (1972). On the other hand, a dominant period should prevail according to Kasahara (1957), Tsujiura (1967), Archambeau (1968) and Linde and Sacks (1971, 1972). In the first case, the constant level in the spectrum is supposed to reflect the moment of the equivalent double couple point source, while in the second case, the dominant period is thought to be a function of the source dimension. The empirical verification of either of the models is overdue, mainly because of the difficulties of obtaining reliable instrument responses at long periods. This limitation is equally faced in the present investigation. Though the spectra do reveal a constant level in part of the frequency range investigated, a subsequent drop at still lower frequencies cannot be excluded. The interpretation of spectra given in the present paper favours models predicting a constant level down to lowest frequencies. The empirical spectra obtained in course of the present study do not preclude however the possibility of the models predicting a dominant period to apply at least to some class of seismic events.

The spectra presented in Figs. 3–6 are corrected for the instrument response and for the geometric spreading of the wave front. They are thus more reliable in the low-frequency part, in the sense that they reflect the spectrum radiated from the source.

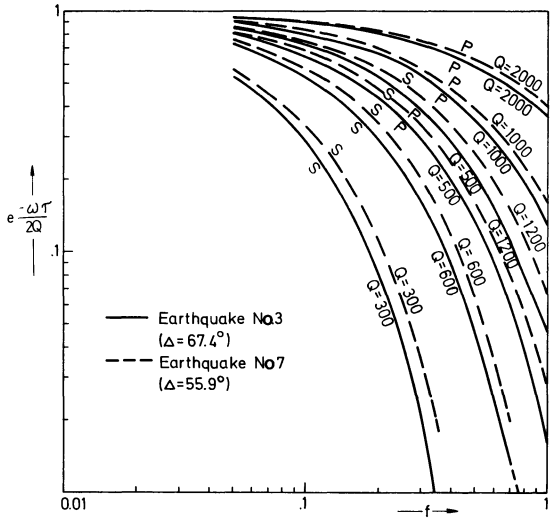

Fig. 9. Absorption effect as a function of frequency for two of the investigated earthquakes. A range of Q-values is assumed for P- and S-waves, as shown

A further correction for the attenuation would have to be applied, particularly in the high-frequency part if a progressive deterioration of reliability with frequency is to be prevented. The correction would require the knowledge of the distribution of the Q-factor along the ray path from the Himalayas to the recording station.

In Fig. 9 the factor is shown, by which the spectral densities of P- and S-waves would have to be divided in the applicable frequency range, for average Q-values along the ray path ranging from 300 to 2000. In Fig. 10a, b, as an example, the spectrum of the earthquake No. 3, as given in Fig. 4, is compensated for the absorption. Thereby three different Q-values are assumed in each case, as applicable for the respective wave. It can be readily seen that high average Q-values lead to only a slight change in the observed spectrum, while a decrease in the average Q-value yields a spectrum which not only progressively deviates from the observed one, but appears to become less reliable. This is due to the fact that Q is not likely to be constant along the ray path. To avoid the related uncertainties, observation of spectra at near epicentral distances are in need. In any case, the level portion of the spectra suffers least from absorption, which fact leaves moment estimates, and estimates of the corner frequency, virtually unaffected.

The problem of a global Q-profile, and of regional perturbations of such a profile, is under investigation since some time. Recently, Anderson and Hart (1978) have published four Q-profiles for S- and for P-waves, on the basis of abundant, world-wide estimates. Their values tend to be generally lower than hitherto believed. The average $\bar{Q}_\beta$ and $\bar{Q}_\alpha$ above the mantle-core boundary for the models SL2, SL3, SL7, and SL8 amounts to 240 and 600 respectively. Both values are in fair agreement with estimates of Nortmann (1977), who finds average Q-values of 300 and 500 resp. underneath the Eurasian continent.

For earthquakes at epicentral distances of about 65°, as in the present investigation, the ray paths have their lowest point at 1,600 km. The Q-profiles of Anderson and Hart predict that in this case the ray paths have longest segments in layers with Q_β close to 400, and Q_α close to 1,000. Thus, it is likely that the waves analysed here were mainly transmitted through layers with Q-values higher than the respective average values. We conclude that estimates of seismic moments and of corner frequencies, as given here, are only mildly distorted by anelasticity.

Moment (as well as magnitude and energy) determinations made at one station suffer from uncertainties due to the radiation pattern. If, however, a double couple source model is assumed, the radiation maxima of both kinds of body waves are rotated by 45° with respect to each other and the maximum of one should coincide with the minimum of the other. Though some information on the tectonic trend in the investigated area is known (Tandon and Srivastava 1975), a transposition of it into the probable orientation of the fault planes of the investigated earthquakes, and a subsequent determination of $R_{\theta\phi}$ [see (1)] is futile in view of other uncertainties. We observe systematically lower values of moments from P-waves, if compared with those from S-waves (see Table 4). Both are, however, always of the same order of magnitude for a given earthquake,

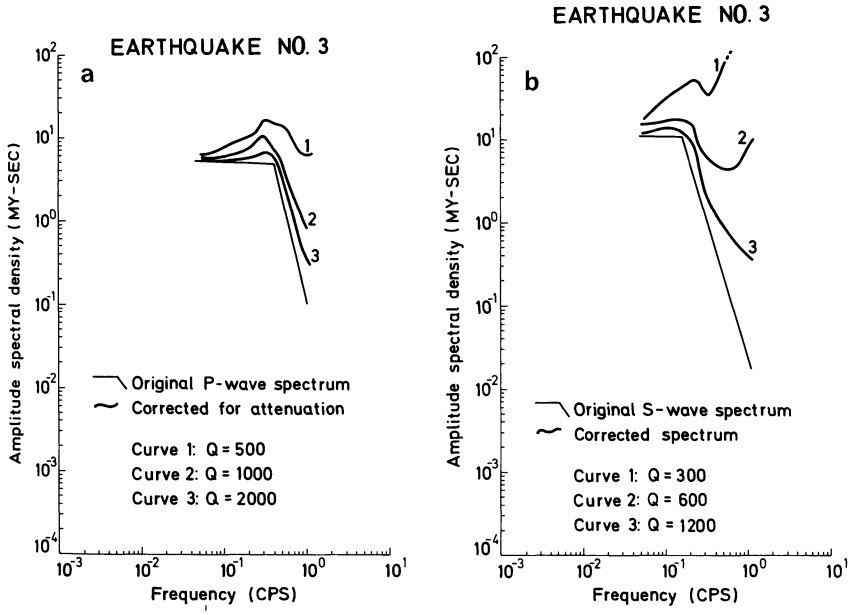

Fig. 10a and b.
Distortion of P-wave spectrum (**a**) and S-wave spectrum (**b**) for earthquake No. 3 (compare Fig. 4). Three different Q-values are assumed, as shown

indicating that the observation is made far away from a nodal line of either the *P*- or the *S*-wave. We consider this fact as justifying the neglection of the radiation pattern in the present case. For numerical calculations $R_{\theta\phi}$ is set equal to one.

The asymptotic behaviour of the spectra at high frequencies is reflected by the γ-coefficient. The numerical values for the eight earthquakes considered are given in Table 3. The averages of γ are 3.8 for *P*-waves and 4.1 for *S*-waves. If high *Q*-values are assumed along the ray path (e.g., 1,200 and 2,000 for *S*- and *P*-waves respectively; see Fig. 10), the observed γ-values can be interpreted in terms of build-up of slip at any point of the fault plane. As pointed out by Savage (1972), γ is determined then by the order of discontinuities in the pulse shape. Discontinuities in the displacement, velocity and acceleration of the initial motion result in $\gamma = 1, 2, 3$ respectively. A $\gamma \cong 4$, as found here, would imply an initial increase with time of the approximate form $t^3 \exp(-vt)$.

It is more likely however, that the γ-values determined from the spectra are influenced not only by the radiated spectrum, but by *Q* along the ray path as well. Whether the radiated spectrum in fact had a $\gamma = 3$, as corresponding to an initial displacement of the form $t^2 \exp(-vt)$ (Savage model), or $\gamma = 2$, corresponding to $t \exp(-vt)$ (Brune and Berckhemer and Jacob model), or even $\gamma = 1$ corresponding to a Heaviside unit step increase, could only be decided if detailed *Q*-values along the ray path were available.

We finally remark that, at variance with Haskell's model, but in agreement with the findings of Wyss and Hanks (1972) and Hanks and Wyss (1972), the corner frequencies for *P*-waves are about twice those for *S*-waves in case of the investigated Himalaya-earthquakes.

Conclusions

1. The spectra of 8 Himalaya-earthquakes are of both one-corner-frequency and two-corner-frequency type. While the fault length exceeds the width in the latter case, both, length and width are comparable in the former case.
2. The earthquakes are found to be of low-moment, low-stress drop type.
3. A discrepancy is seen between the fault plane areas as determined from the spectra and from the aftershock distribution for earthquakes with magnitudes above 6.4, but in agreement for lower magnitudes. From this, an only partial strain release is concluded in the large-magnitude earthquakes, which usually are followed by long aftershock sequences.
4. The stress drop and the fault length show only an unconspicuous dependence on magnitude.
5. Assuming no absorption losses along the ray path, the asymptotic behaviour of the spectra suggests an initial displacement proportional to $t^3 \exp(-vt)$.

Acknowledgement. The research was carried out while one of the authors (S.K.U) was an awardee of a fellowship of Alexander von Humboldt Foundation, Bonn-Bad Godesberg (FRG). The author expresses his thanks to the Director of the Institute of Geophysics, Hamburg University, Professor Dr. H. Menzel, for providing facilities to carry out the work.

Dipl. Geoph. R. Nortmann from the Institute of Geophysics, Hamburg University, made available some of his computer programmes. The basic data for the research were provided by the Central Seismological Observatory, Erlangen. Part of the research was performed under a grant of Deutsche Forschungsgemeinschaft, Bonn-Bad Godesberg.

All support is gratefully acknowledged.

References

Aki, K.: Generation and propagation of *G* waves from the Niigata earthquake of June 16, 1964. Part 2: Estimation of earthquake moment, released energy and stress-strain drop from the *G* wave spectrum. Bull. Earth. Res. Inst. **44**, 73–88, 1966

Aki, K.: Scaling law of seismic spectrum. J. Geophys. Res. **72**, 1217–1231, 1967

Aki, K.: Seismic displacements near a fault. J. Geophys. Res. **73**, 5359–5376, 1968

Aki, K.: Scaling law of earthquake source time function. Geophys. J. R. Astron. Soc. **31**, 3–25, 1973

Anderson, D.L., Hart, R.S.: *Q* of the Earth. J. Geophys. Res. **83**, 5869–5882, 1978

Archambeau, C.B.: General theory of elastodynamic source fields. Rev. Geophys. Space Phys. **6**, 241–288, 1968

Båth, M.: Spectral Analysis in Geophysics. Amsterdam, Oxford, New York: Elsevier Scientific Publishing Company 1974

Båth, M., Duda, S.J.: Earthquake volume, fault plane area, seismic energy, strain, deformation and related quantities. Ann. Geofis. **17**, 353–368, 1964

Ben-Menahem, A.: Radiation of seismic body waves from a finite moving source in the earth. J. Geophys. Res. **67**, 345–350, 1962

Berckhemer, H., Jacob, K.H.: Investigation of the dynamical process in earthquake foci by analyzing the pulse shape of body waves. Bericht des Institutes für Meteorologie und Geophysik der Universität Frankfurt/Main, Nr. 13, 1968

Brune, J.N.: Tectonic stress and the spectra of seismic shear waves from earthquakes. J. Geophys. Res. **75**, 4997–5009, 1970

Byerly, P., DeNoyer, J.: Energy in earthquakes as computed from geodetic observations. Contribution to Geophysics in honour of B. Gutenberg; H. Benioff et al. (eds.): pp. 17–35. New York: Pergamon Press 1958

Chinnery, M.A.: The deformation of the ground around surface faults. Bull. Seismol. Soc. Am. **51**, 355–372, 1961

Chinnery, M.A.: The stress changes that accompany strike slip faulting. Bull. Seismol. Soc. Am. **53**, 921–932, 1963

Chinnery, M.A.: Earthquake magnitude and source parameters. Bull. Seismol. Soc. Am. **59**, 1909–1982, 1969

Hanks, T.C., Wyss, M.: The use of the body wave spectra in the determination of seismic source parameters. Bull. Seismol. Soc. Am. **62**, 561–589, 1972

Haskell, N.A.: Total energy and energy spectral density of elastic wave radiation from propagating faults. Part I: Bull. Seismol. Soc. Am. **54**, 1811–1841, 1964. Part II: Bull. Seismol. Soc. Am. **56**, 125–140, 1966

Haskell, N.A.: Elastic displacements in the near field of a propagating fault. Bull. Seismol. Soc. Am. **59**, 865–908, 1969

Hirasawa, T., Stauder, W.: On seismic body waves from a finite moving source. Bull. Seismol. Soc. Am. **55**, 237–262, 1965

Iida, K.: Earthquake energy and earthquake faults. J. Earth. Sci. Nagoya Univ. **7**, 98–107, 1959

Kasahara, K.: The nature of seismic origins as inferred from seismological and geodetic observations. Bull. Earth. Res. Inst. Tokyo Uni. **35**, 473–532, 1957

Keilis-Borok, V.I.: An estimation of the displacement in an earthquake source and of the source dimensions. Ann. Geofis. **12**, 205–214, 1959

Linde, A.T., Sacks, I.S.: Errors in the spectral analysis of long period seismic body waves. J. Geophys. Res., **76**, 3326–3336, 1971

Linde, A.T., Sacks, I.S.: Dimension, Energy and Stress release for South American deep earthquakes. J. Geophys. Res. **77**, 1439–1451, 1972

Nortmann, R.: Die Anelastizität des Erdmantels im Europäischen Raum, Diplomarbeit, Institut für Geophysik der Universität Hamburg, Dezember 1977

Press, F.: Dimension of the source region for small shallow earthquakes, Proceedings of the Vesiac Conference on the current status, and future progress for understanding the source mechanism of shallow seismic events in the 3 to 5 magnitude range, 1965

Reid, H.: The mechanism of earthquakes; California earthquake of April 8, 1906, Report of State Investigation Commission (Carnegie Institution of Washington), Vol. 2, 1910

Savage, J.C.: Radiation from a realistic model of faulting. Bull. Seismol. Soc. Am. **56**, 577–592, 1966

Savage, J.C.: Relation of corner frequency to fault dimensions. J. Geophys. Res. **77**, 3788–3795, 1972

Shimshoni, M., Ben-Menaham, A.: Computation of the divergence coefficient for seismic phases. Geophys. J. R. Astron. Soc. **21**, 285–294, 1970

Tandon, A.N., Srivastava, H.N.: Fault plane solutions as related to known geological faults in and near India. Ann. Geofis. **28**, 13–27, 1975

Tocher, D.: Earthquake energy and ground breakage. Bull. Seismol. Soc. Am. **48**, 147–173, 1958

Tsuboi, C.: Deformation of the earth crust as disclosed by geodetic measurements. Beitr. Geophys., Ergeb. Kosm. Phys. **4**, 106–168, 1939

Tsujiura, M.: Frequency analysis of seismic waves, 2. Bull. Earth. Res. Inst. Tokyo Univ. **45**, 973–995, 1967

Wyss, M., Hanks, T.C.: The source parameters of the San Fernando earthquake inferred from teleseismic body waves. Bull. Seismol. Soc. Am. **62**, 591–602, 1972

Received May 22, 1979; Revised Version February 7, 1980